Design Analysis and Performance Optimization of a Lyot Filter for Semiconductor Optical Amplifier Pattern Effect Suppression

Zoe V. Rizou, Kyriakos E. Zoiros, Antonios Hatziefremidis, *Member, IEEE*, and Michael J. Connelly, *Member, IEEE*

***Abstract*—In this paper, we analyze in detail, based on numerical modeling, the use of a Lyot filter to suppress the semiconductor optical amplifier (SOA) pattern effect. By formulating a robust design strategy, which is based on defining appropriate figures of merit and making the necessary tradeoffs between them, the filter performance can be optimized in terms of the wavelength spacing and detuning of its spectral response. The results obtained from this design procedure agree with experiment and enable us to accurately quantify to what degree the Lyot filter can resolve the SOA pattern effect problem.**

***Index Terms*—Lyot filter, numerical modeling, pattern effect, semiconductor optical amplifier (SOA).**

I. Introduction

SEMICONDUCTOR optical amplifiers (SOAs) have technologically matured to such degree that they are widely recognized as key elements for the implementation of optical communications circuits, systems, and networks [1]–[3]. Owing to their multifunctional capability, low power consumption, compactness, broad gain bandwidth, and ability for integration with affordable cost, SOAs constitute a competent solution over existing amplifier alternatives [4]. These distinctive properties have revived interest for direct signal amplification purposes, which have traditionally been the primary target of SOAs [5]. Thus, intense research activity has been reported on the exploitation of SOAs as booster amplifiers, in-line amplifiers, and preamplifiers [6]–[11]. However, the efforts toward this goal are hindered by the pattern effect, which is caused by the strong saturation and incomplete recovery of the SOA gain in between excitation input pulses [1]. The undesirable consequence of this drawback is that the SOA output is determined not only by the current input but also by the history of the SOA gain response to previous inputs. This results in pulse-to-pulse amplitude fluctuations or waveform distortion, depending on whether the pulse occupies a fraction or the whole interval of the bit slot, respectively [12], [13]. Therefore, the SOA can serve as a linear amplifier only if the launched data pulses have a power well below the SOA heavy saturation region, and when they are return-to-zero (RZ) coded, their width is appreciably shortened [14]. The practical merit of this combined action is very limited because it deteriorates the optical signal-to-noise ratio (OSNR), it impedes the maximization of the output power, it results in closer amplifier spacings, and it narrows the input power dynamic range (IPDR) [5]. Furthermore, it makes pulse generation more challenging [15], and it increases the sensitivity to nonlinear effects [16] and intraband phenomena [17]. This clearly designates that other solutions must be used in order to greatly reduce the SOA pattern effect.

Various methods have been proposed to accelerate or compensate for the inherently slow SOA gain recovery. These are based on intervening in the bias current [18] and the dimensions of the active region [18], [19], applying external [8], [20] or internal [21], [22] assist light, and using special coding [23], active interferometric arrangements [24], [25] as well as new materials [26], [27]. However, for data rates exceeding 10 Gb/s, these options may not be the best to adopt. There are several reasons responsible for this fact. These include the lack of flexibility in manipulating the gain [21], [22], the degradation of the quality of the amplified pulses [18], the disturbance of fundamental SOA physical properties [19], the supply and control of extra high power [8], [20], [28], the precise phase adjustment [24], the employment of sophisticated data modulation formats [23], the use of an extra SOA stage [8], the tight operation settings of tricky architectures that exploit nonlinear effects [25], and dealing with devices of different fabrication and dynamical behavior than usual [26], [27].

On the other hand, and thanks to its passive nature, optical filtering seems to be more appropriate as it is a relatively simple scheme [29]–[35]. This technique relies on suppressing the components of the pulse spectrum that have been shifted to longer wavelengths due to the irregular SOA gain variation [29]. The Lyot filter falls into this category and we have recently shown how it can be used to suppress the SOA pattern effect induced on 10-Gb/s RZ data pulses [33]. However, the original aim of this experiment was to confirm the feasibility of employing this type of filter rather than trying to optimize its performance. In this paper, we present a comprehensive simulation analysis, which is

Manuscript received November 26, 2012; revised January 25, 2013 and February 19, 2013; accepted February 21, 2013. This work was supported in part by national research project Massive implemented through the Operational Program "Education and Lifelong Learning" and cofinanced by the European Union (European Social Fund) and Greek national funds.

Z. V. Rizou and K. E. Zoiros are with the Department of Electrical and Computer Engineering, Democritus University of Thrace, Xanthi 67100, Greece (e-mail: zoirizo@ee.duth.gr; kzoiros@ee.duth.gr).

A. Hatziefremidis is with the Department of Aircraft Technology, Technological Educational Institute of Chalkis, Chalkis 34400, Greece (e-mail: ahatzi@teihal.gr).

M. J. Connelly is with the Department of Electronic and Computer Engineering, University of Limerick, Limerick, Ireland (e-mail: michael.connelly@ul.ie).

Digital Object Identifier 10.1109/JSTQE.2013.2250258

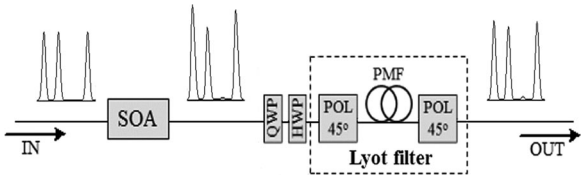

Fig. 1. Block diagram of an SOA and Lyot filter under study. SOA: semiconductor optical amplifier, QWP: quarter-wave plate, HWP: half-wave plate, PMF: polarization maintaining fiber, POL 45°: polarizer aligned at 45° with respect to the axes of the PMF.

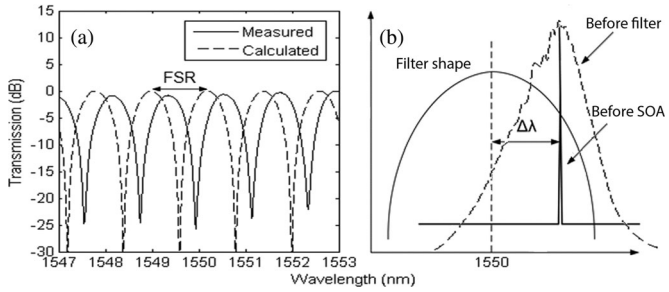

Fig. 2. (a) Measured (solid line) and calculated (dashed line) Lyot filter power spectral response with FSR indicated. (b) Magnified lobe (solid line) of (a), which schematically shows the transmission peak detuning $\Delta\lambda$ required for filtering the broadened spectrum of the amplified data (dashed line) to suppress the SOA pattern effect.

conducted in order to thoroughly assess the impact of the critical Lyot filter parameters on important figures of merit. By using numerical modeling, we confirm the experimental results and further quantify the significant performance improvements realized by the Lyot filter compared to the SOA alone. The model leads to the extraction of useful guidelines for the optimum design of the Lyot filter when employed for SOA pattern effect suppression.

The remainder of this paper is organized as follows. In Section II, we explain how the SOA pattern effect can be suppressed by means of a Lyot filter. In Section III, we formulate the model that is applied to describe the operation of the concatenated SOA and Lyot filter in the time and frequency domain. In Section IV, we present an extensive set of simulation results that enable us to specify the permissible range and optimum values of the critical performance parameters. Also, we fully characterize the capability of the Lyot filter to suppress the SOA pattern effect. Finally, in Section V, we summarize the main benefits offered by the Lyot filter for SOA pattern effect suppression.

II. Principle of SOA Pattern Effect Suppression Using the Lyot Filter

Fig. 1 illustrates the block diagram of the configuration under study, which consists of a Lyot filter serially connected to an SOA. A data signal is inserted in the SOA with power and temporal content that saturates strongly the SOA. Under these operating conditions, and since the SOA gain recovery time is finite, the SOA gain dynamics are not perturbed in a uniform manner but depend on the input data pattern [1]. As a consequence, the amplified pulses experience significant amplitude variations and are spectrally broadened due to self-phase modulation (SPM), which red shifts their peak wavelength [12], [36]. However, if this uneven red shift could be reduced, then the pattern effect would be compensated [29]. For this purpose, the distorted data sequence is launched into a Lyot filter whose structure is shown in Fig. 1. The bulk implementation of this passive module comprises of a section of polarization maintaining fiber (PMF), which is sandwiched between two polarizers (POL) aligned at 45° with respect to the birefringent axes of the PMF. Directly before the first polarizer, quarter and half-wave plates (QWP, HWP) are inserted to ensure favorable alignment of the incoming modulated light's state of polarization. Due to the different propagation constants of the two axes of the PMF, the intensity transmission of the Lyot filter has a wavelength-dependent periodic comb-like profile. This is shown in Fig. 2(a), in which both measured and simulated power transfer functions have been plotted. The two curves are not exactly the same because the experimental one has been obtained by injecting a C-band light source into the stand-alone Lyot filter [33]. Therefore, the quality of the outcome, which is monitored in an optical spectrum analyzer (OSA), depends on the real measurement conditions. Thus, the components that construct the Lyot filter are not lossless, the rotating elements are manually controlled at the cost of limited precision, the PMF is sensitive to the environmental changes, and the OSA has a finite dynamic range. For these practical reasons, there exist some differences against the theoretical transfer function. More specifically, the magnitudes of the peaks as well as of the peak-to-notch contrast ratio are smaller and the transmission at the notches is not uniform. There is also a slight deviation in the position of the peaks and notches. This is attributed to the fact that the experimental data acquired through the OSA are processed in LabVIEW software. In contrast, the theoretical data are sampled and undergo fast Fourier transform (FFT) in MATLAB software assuming ideal components for the case of the optimized Lyot filter. Still the theoretical and the experimental results are well matched since both curves have the same form and consist of alternating maxima and minima, with the notches situated midway between adjacent peaks. The wavelength spacing between these peaks or free spectral range (FSR) is given by $\mathrm{FSR} = \lambda^2/(BL)$, where λ is the reference wavelength, B the birefringence, and L the length of the PMF [33], [37]. Owing to these transfer function characteristics, we can exploit the Lyot as a notch filter to cancel the spread of the spectral components toward the longer sideband and subsequently the associated pattern-dependent degradation. This can be achieved if the transmission peak of the Lyot filter's spectral response is set at a lower point than the wavelength of the optical data carrier, so that the transmittance is decreased as the wavelength is increased [30], [32]. This is schematically shown in the magnified lobe of Fig. 2(b), where the transmission peak detuning to the blue side of the signal spectrum is denoted by $\Delta\lambda$. Consequently, the asymmetrically broadened spectral components after the SOA [see Fig. 2(b)] are forced to lie around the notches and are suppressed in proportion to the degree of their red shift. If used in this manner, the Lyot filter can greatly reduce the SOA pattern effect and restore the quality

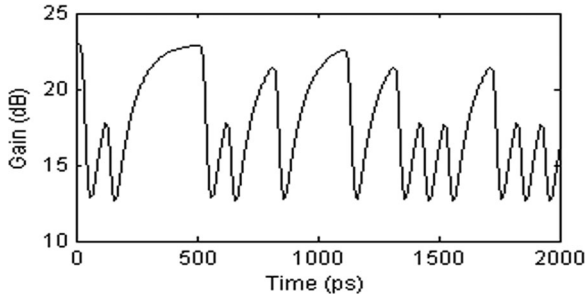

Fig. 3. Instantaneous SOA gain variation in response to the exemplary data frame "11000110100101110111."

of the amplified data stream. The spectral manipulation required to achieve this goal involves properly choosing and controlling the wavelength spacing and detuning of the Lyot filter, as we discuss in Section IV-A.

III. Simulation

The simulation of the operation of the joint SOA and Lyot filter configuration relies on mathematically expressing the temporal and spectral output after each one of these elements. Starting with the SOA, the signal power P and power spectrum S of the amplified pulses are given by

$$P_{\mathrm{SOA}}(t) = |E_{\mathrm{SOA}}(t)|^2\,,\ S_{\mathrm{SOA}}(\lambda) = |F\left[E_{\mathrm{SOA}}(t)\right]|^2 \quad (1)$$

where F denotes FFT and $E_{\mathrm{SOA}}(t)$ is the electric field of the amplified data, which is normalized so that its square modulus represents power [36]. $E_{\mathrm{SOA}}(t)$ can be expressed as

$$E_{\mathrm{SOA}}(t) = E_{\mathrm{data}}(t)\exp\left[\tfrac{1}{2}(1-\mathrm{j}\alpha)\,h(t)\right] \quad (2)$$

where α is the SOA linewidth enhancement factor and $h(t)$ is the integrated SOA power gain in response to data of amplitude $E_{\mathrm{data}}(t)$ [36]. $h(t)$ obeys the following differential equation:

$$\frac{dh(t)}{dt} = \frac{\ln(G_{ss}) - h(t)}{\tau} - \frac{|E_{\mathrm{data}}(t)|^2}{E_{\mathrm{sat}}}\left\{\exp\left[h\left(t\right)\right] - 1\right\} \quad (3)$$

where G_{ss}, τ, and E_{sat} are the SOA small signal single-pass gain, carrier lifetime, and saturation energy, respectively [36]. In order to calculate $h(t)$, we take into account the heavy strain imposed on the SOA gain dynamics not only by the power of the data pulses, $P_{\mathrm{data}}(t) = |E_{\mathrm{data}}(t)|^2$, but also by their temporal content [38]. This fact dictates that (3) is numerically solved as outlined in [38], which is done by using the following fixed parameters values: $G_{ss} = 23\,\mathrm{dB}, \tau = 75\,\mathrm{ps}, E_{\mathrm{sat}} = 1.5\,\mathrm{pJ}$, and $\alpha = 8$ [33]. The input data signal is a Gaussian-shaped, 10-Gb/s, unchirped, RZ, 2^7–1 bit-long pseudorandom binary sequence (PRBS). The marks of this stream have a peak power of 4.6 mW and are 20 dB stronger than the spaces, while their temporal and spectral full-width at half-maximum is 27 ps and 0.13 nm, respectively. These pulses saturate strongly the SOA and provoke a noticeable pattern effect at its output [38]. Fig. 3 shows indeed that the instantaneous SOA gain variation due to the random data stream is significant.

On the other hand, the field transfer function of the Lyot filter is

$$T_{\mathrm{Lyot}}(\lambda) = \frac{1}{2}\left\{1 + \exp\left[j2\pi\left(\frac{BL}{\lambda} - \frac{\Delta\lambda}{\mathrm{FSR}}\right)\right]\right\} \quad (4)$$

where we use $B = 4\times10^{-4}$ in our simulation analysis [37]. The negative detuning $\Delta\lambda$ of the Lyot filter from the wavelength of the optical data carrier can be varied up to 50% of the wavelength spacing between transmission maxima, i.e., $0 \le \Delta\lambda \le \mathrm{FSR}/2$ [37]. The electric field at the output of the Lyot filter is given by

$$E_{\mathrm{Lyot}}(t) = F^{-1}\left\{F\left[E_{\mathrm{SOA}}(t)\right]T_{\mathrm{Lyot}}(\lambda)\right\} \quad (5)$$

where F^{-1} denotes inverse fast Fourier transform (IFFT). Therefore, the signal power at the output of the Lyot filter is $P_{\mathrm{Lyot}}(t) = |E_{\mathrm{Lyot}}(t)|^2$ and the power spectrum is $S_{\mathrm{Lyot}}(\lambda) = |F\left[E_{\mathrm{Lyot}}(t)\right]|^2$. The functions described by (1)–(5), including the required FFT and IFFT operations, are implemented using MATLAB software.

IV. Results and Discussion

A. Selection of Lyot Filter Attributes

In order to analyze the performance of the Lyot filter, we have to set the criteria against which this task will be accomplished. The degree of amplitude modulation (AM) of the output signal has been widely adopted for this purpose [24], [32]–[35], [38]. This metric is defined as $\mathrm{AM(dB)} = 10\log\left(P^1_{\max}/P^1_{\min}\right)$, where $P^1_{\max}$ and $P^1_{\min}$ are the maximum and minimum peak powers of the marks in the amplified data stream. Ideally, the AM must be as low as possible. Although the AM allows us to quantify the pattern-dependent pulse-to-pulse wandering, it does not cover other negative consequences of the pattern effect. In particular, due to Lyot filtering, a portion of useful power contained in the suppressed red-shifted spectral components is inevitably lost [33]. This in turn causes the data sequence to receive less amplification than after the SOA alone. This reduction in the output power is an amplification penalty [8] that cannot be ignored but must be taken into account through the index

$$G_{\mathrm{ar}}(\mathrm{dB}) = \left|P^{\mathrm{avg}}_{\mathrm{out,Lyot}}\,(\mathrm{dBm}) - P^{\mathrm{avg}}_{\mathrm{out,SOA}}\,(\mathrm{dBm})\right| \quad (6)$$

where the subscript "ar" stands for "$a$mplification $r$eduction" and $P^{\mathrm{avg}}_{\mathrm{out,SOA}}$ and $P^{\mathrm{avg}}_{\mathrm{out,Lyot}}$ are the total average powers at the SOA and Lyot filter output, respectively. In this definition, the insertion loss of the Lyot filter is incorporated in $P^{\mathrm{avg}}_{\mathrm{out,Lyot}}$. This happens because in the experiment, this loss is fully compensated by a linear amplifier placed at the exit of the Lyot filter [33]. Since our simulation analysis aims at reproducing the experimental conditions as realistically as possible, this loss is not taken explicitly into account. On the other hand, it is known that the filtering schemes which rely on intensity [12], [38] or polarization [33], [34] discrimination can distort the profile of the amplified pulses. Thus, for a complete characterization of the Lyot filter's capability to suppress the SOA pattern effect, we must take AM, G_{ar}, and the pulse profile simultaneously into account. This capability depends on the way the Lyot filter's spectral response is configured by means of FSR and $\Delta\lambda$. In the

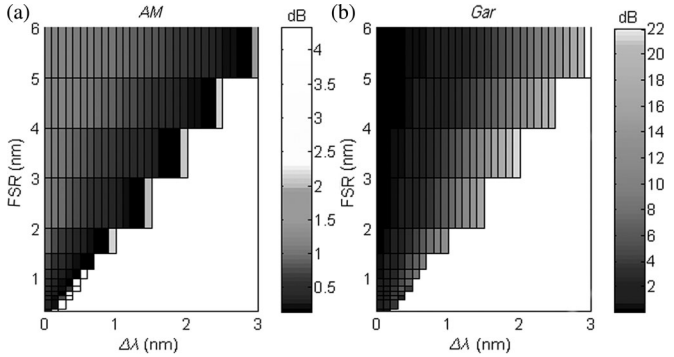

Fig. 4. Variation of (a) AM and (b) SOA-Lyot filter amplification reduction $G_{\rm ar}$ versus FSR and detuning of the Lyot filter's spectral response.

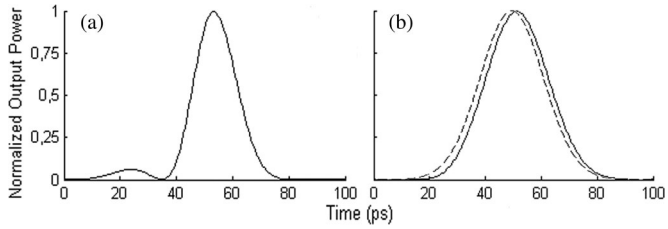

Fig. 5. Profile of isolated data pulse at Lyot output for (a) nonproperly selected and (b) optimized filter parameters (solid line). The profile of the same data pulse at the SOA input is also shown in (b) (dashed line) for comparison.

following, we present simulation results aiming at studying the impact of these parameters and suitably selecting them so that all defined performance criteria can be met.

Fig. 4(a) shows the AM as a function of FSR and $\Delta\lambda$. The diagram has the form of a grid where the AM that results for each combination of FSR and $\Delta\lambda$ is depicted with a different shade according to the gradation in the adjacent climax. The scanned range of the FSR is chosen so that the lower bound corresponds to a PMF length of approximately 15 m, which is a reasonable length for a Lyot filter constructed in the laboratory [33]. The upper bound allows us to monitor the change of the defined performance criteria to an extent that the influence of the FSR on them can be thoroughly evaluated. This affects the maximum possible variation of $\Delta\lambda$, which must not exceed FSR/2.

From Fig. 4(a), we can make some important observations. First, with no detuning, i.e., $\Delta\lambda = 0$ nm, the AM is improved as the FSR is decreased. This happens because with this change, the Lyot filter can compensate for the pattern effect more efficiently. More specifically, the wavelength spacing of its transfer function is reduced and so the central wavelength of the input data is more likely to be located closer to one of the transmission peaks. In this manner, this spectral component can pass through the Lyot filter with the least possible magnitude impairment [30]. This condition is necessary when employing filtering techniques for restoring amplified signals [32]. Furthermore, the negative slope of the spectral lobes is made steeper for a lower FSR, and so the red-shifted spectral components can fall closer to the notches. This in turn enables these components to be attenuated in direct analogy to the degree of their shift, which is required for efficient pattern effect suppression. Second, the introduction of wavelength detuning shifts the AM to lower values. The AM is minimized when $\Delta\lambda$ tends to, but does not reach, its upper bound, i.e., FSR/2. This designates that the role of $\Delta\lambda$ in mitigating the pattern effect is decisive since, compared to $\Delta\lambda = 0$ nm, the AM is further improved. However, there exist many FSR and $\Delta\lambda$ pairs for which the AM is tolerable. Nevertheless, we can limit the permissible sets of FSR and $\Delta\lambda$ by considering the impact of these parameters on $G_{\rm ar}$. For this purpose, we see from Fig. 4(b) that the combinations of the FSR and $\Delta\lambda$ which reduce the AM have an opposite effect on $G_{\rm ar}$. This means that a tradeoff must be made between the amplification reduction of the SOA-Lyot filter system and the degree of pattern effect reduction [8], [24], [25], [32]–[35]. This tradeoff is efficiently achieved for FSR $\leq$ 1.5 nm and $\Delta\lambda \leq$ FSR/4, since the AM and $G_{\rm ar}$ are kept below the typical limits of 1 dB and 4 dB, respectively [8], [12]. Then, the remaining FSR–$\Delta\lambda$ pairs are those that allow the data pulses to retain their initial shape and not become distorted. For example, the pair FSR $= 0.6$ nm, $\Delta\lambda = 0.1$ nm, is not appropriate since, as shown in Fig. 5(a), a satellite pulse appears inside the bit slot of the amplified pulses and distorts their profile. Therefore, and after systematically following the proposed design procedure, we can deduce the optimum values for the FSR and $\Delta\lambda$. These are FSR $= 1.2$ nm within a range of ± 0.35 nm, and $\Delta\lambda = 0.2$ nm $\sim$ FSR/6. This combination results in the acceptable AM $= 0.3$ dB, as opposed to AM $= 1.22$ dB without the Lyot filter, and $G_{\rm ar} = 2.7$ dB. This amplification reduction is also acceptable from a system perspective since the SOA provides a much greater average gain. In fact, this quantity, which is defined as

$$G_{\rm avg,SOA}({\rm dB}) = P^{\rm avg}_{\rm out,SOA}\,({\rm dBm}) - P^{\rm avg}_{\rm in,SOA}\,({\rm dBm}) \qquad (7)$$

where $P^{\rm avg}_{\rm in,SOA}$ is the average power of the PRBS inserted in the SOA, equals 12.2 dB for the conditions that the SOA is biased to operate. On the other hand, by combining (6) and (7), the net gain of the SOA-Lyot filter system can be expressed as [38]

$$G_{\rm net}({\rm dB}) = G_{\rm avg,SOA}({\rm dB}) - G_{\rm ar}({\rm dB}) \qquad (8)$$

and equals 9.5 dB. This net gain is sufficient for direct signal amplification during experiments since, as mentioned before, the insertion loss of the Lyot filter is compensated by an extra booster amplifier [33]. However, without this external assistance, the net gain is smaller. Still this reduction in the net gain can be compensated if we use an SOA of higher small signal gain. As it will be shown in Section IV-B [see Fig. 8(a)], the performance of the optimized SOA-Lyot filter scheme in terms of the AM and $G_{\rm ar}$ is not impaired if the SOA small signal gain is increased. Physically, a higher small signal gain makes the instantaneous SOA gain variations occur around a higher average level. This is translated into a higher SOA average gain and accordingly into a higher net gain. Thus, if we increase the SOA small signal gain from 23 to 29 dB, the net gain is increased too, by 4 dB. Then, if we account for the insertion loss of the Lyot filter [33], the remaining net gain is of the order of 5.5 dB. This amount is sufficient for loss compensation in a 17-km standard single-mode fiber link with dispersion compensation. This length implies that the SOA-Lyot filter system can support 10-Gb/s data amplification with suppressed pattern

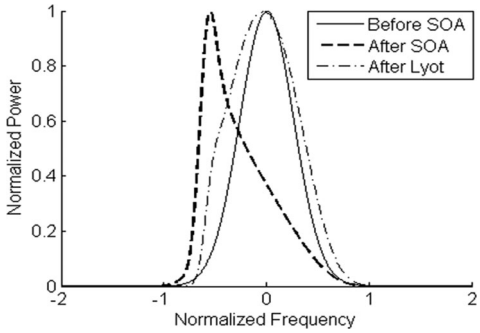

Fig. 6. Power spectra at SOA input (solid line), SOA output (dashed-bold line) and Lyot output for optimized filter parameters (dashed-dotted line).

effects in short-haul fiber optic communication networks. Finally, the quality of the data pulses is preserved. This can be seen in Fig. 5(b), where we depict an isolated data pulse at the output of the Lyot filter together with its counterpart at the SOA input. Clearly, the profiles of the two data pulses are identical and their envelopes are nearly superposed. Also, it is worth mentioning that the FSR employed in the experimental demonstration [33] is included among the numerically specified values of this parameter, which supports the validity of the derived results.

Using the optimized Lyot filter, the central peak of the pulse spectrum that is broadened at the SOA output [36] is brought by the Lyot filter back to almost its original position. This can be seen in Fig. 6 for the mark that follows after six consecutive spaces and hence is mostly prone to the pattern effect inside the amplified data stream. The obtained spectra are in agreement with the experimental evidence in terms of both form and peak shift [33]. However, the time-bandwidth product at the output of the SOA-Lyot combination is over the minimum for Gaussian-shaped pulses, which means that the pulses become chirped [39]. This happens when filtering schemes of the same type as in [38] are used to suppress the SOA pattern effect. The Lyot filter is an implementation in the polarization domain that lies in this category. According to [38], it cannot fully eliminate the SPM-induced red chirp, which is associated with the SOA pattern effect, but only reduce the variations of its unequal peaks. Thus, in order to avoid disturbing the performance of next SOA-Lyot stages, this residual chirp must not be allowed to broaden the forwarded pulses beyond their pulsewidth at the input of the first stage. Otherwise, the pattern effect will be aggravated due to the slower SOA response to pulses of longer duration [14]. Then, the optimized Lyot filter will not be able to suppress the pattern effect as efficiently as in the first stage. This necessary condition can be satisfied if the pulses after the Lyot filter are compressed by compensating for their chirp in a standard single-mode fiber so as to become again transform limited [39]. The requirements in order for this chirp compensation to be possible [38] also hold in our case. In fact, the pulses at the output of the Lyot filter are Gaussian shaped, while the variation of the chirp over their central part is linear. This is confirmed from Fig. 5(b) as well as from the evidence available on the chirp profile when suppressing the SOA pattern effect, using the same concept

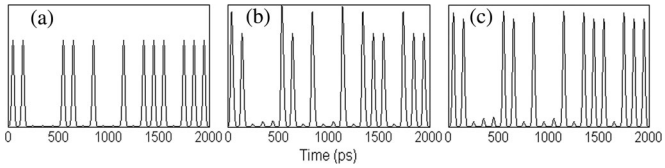

Fig. 7. Simulated temporal waveforms at (a) SOA input, (b) SOA output, and (c) Lyot output for optimized filter parameters.

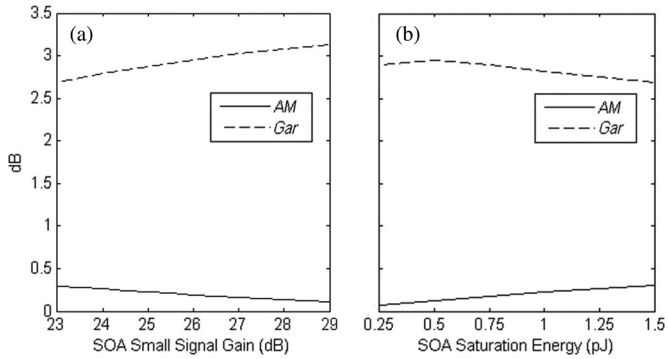

Fig. 8. Variation of AM and $G_{\rm ar}$ at optimized Lyot filter output versus (a) SOA small signal gain and (b) saturation energy.

of spectral elimination, on pulses which are affected only by interband [39] and not intraband [35] phenomena.

B. SOA-Lyot Filter Performance for Ideal Signals

By following the design rules extracted in the previous section for choosing the FSR and $\Delta\lambda$, it is possible to sufficiently suppress the SOA pattern effect. This is shown in Fig. 7 for the representative 20-bit-long data frame in Fig. 7(a). The intense peak fluctuations between the amplified "1"s observed in Fig. 7(b) are greatly equalized in Fig. 7(c) by the optimized Lyot filter. This improvement is quantified by the drop in the AM from over 1 dB after the SOA to 0.28 dB after the Lyot filter, at the expense of 2.7 dB amplification reduction. These numerically obtained values are comparable to those reported in [33], which indicates that the agreement between theory and experiment is very good. They are also robust against changes of the parameters that determine the output of the SOA through (2) and (3). For example, if the SOA small signal gain is increased and the saturation energy is decreased, the AM remains acceptable and $G_{\rm ar}$ can be still compensated, as it can be seen in Fig. 8(a) and (b), respectively.

The performance of the optimized Lyot filter for longer PRBS is similar to that obtained for the 2^7–1-bit-long PRBS. The evaluation criterion used in this case is the AM between the "1" that follows after the longest string of repeated "0"s and the "1" that appears just before this run but also after the same number of consecutive "1"s. Thus, we have found that there are no substantial differences in the reduction of the AM even for PRBS lengths 2^9–1 and 2^{11}–1. Physically, this happens because, according to Fig. 3, the number of consecutive marks required for the SOA to reach saturation equilibrium is lower than the corresponding run length of the considered PRBS [40].

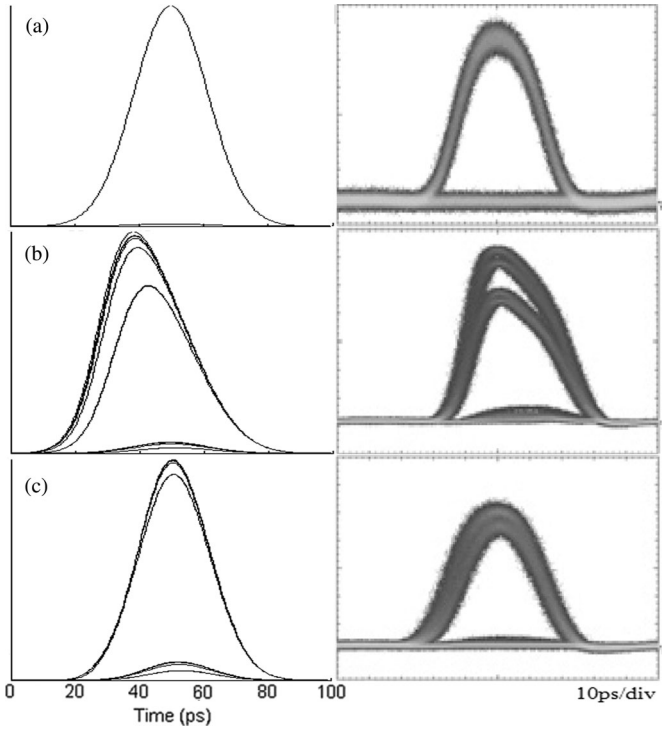

Fig. 9. Eye diagrams at (a) SOA input, (b) SOA output, (c) Lyot output for optimized filter parameters. Left column: Simulation results. Right column: Experimental results [33].

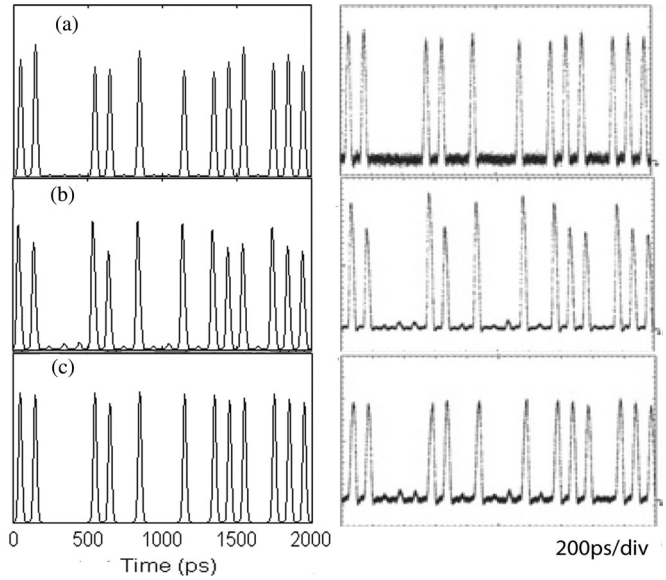

Fig. 10. Temporal waveforms for data pulses with initial pattern effect at (a) SOA input, (b) SOA output, and (c) Lyot output for optimized filter parameters. Left column: Simulation results. Right column: Experimental results [33].

In Fig. 9, we monitor the pseudoeye diagrams [41] and evaluate the impact on the extinction ratio (ER) [42] after the SOA and after the Lyot filter. The simulation results (left column) show that the change in the quality of the eye diagram complies with the trend of the experimental results (right column) [33]. More specifically, the eye diagram at the SOA output is degenerated and comprises of asymmetric subenvelopes [see Fig. 9(b)]. However, with the addition of the optimized Lyot filter, more traces of "1"s are superimposed on top of each other within the same bit slot, while the vertical distance between them becomes smaller [see Fig. 9(c)]. Thus, the eye diagram is reshaped and resembles that at the input of the SOA [see Fig. 9(a)]. The ERs have a similar behavior since their initial high level of 20 dB, which is degraded to 10.9 dB, is restored to 17.2 dB. These numerically calculated values are very close to the experimental ones reported in [33].

C. SOA-Lyot Filter Performance for Nonideal Signals

In this section, we assess whether the designed Lyot filter can reduce the AM that already exists on the data pulses before they enter the SOA, which is a critical capability when cascading many SOAs [43], [44]. In fact, even if the AM of these pulses at the output of a single SOA is acceptable, their peak amplitude difference is not fully extinguished and hence it can accumulate between amplification stages. This in turn may degrade the irregular SOA gain saturation and progressively increase the AM in a chain of SOAs. The placement of a Lyot filter after each SOA can help prevent the pattern effect from scaling from one SOA to the other much beyond its acceptable level. From a physical perspective, this is possible because due to SPM, the spectrum of the stronger input marks is more broadened to longer wavelengths than that of the weaker ones. Thus, the red-shifted components of the higher amplitude marks fall closer to the notches than those of the lower marks. As a result, the Lyot filter allows a larger fraction of the spectrum to pass for the less intense marks. In this manner, the higher marks are clamped and the lower ones are enhanced, which balances their peak variations. This regenerating effect achieved at the output of the Lyot filter is depicted in Fig. 10. The AM of the input data stream [see Fig. 10(a)] has a profile that resembles the experimental one [33] but a higher level of 1 dB. From this figure, we see that due to the incomplete recovery of the SOA gain in between excitation pulses the initial AM cannot be compensated simply by gain modulation [44]. Consequently, the AM is transferred at the SOA output [see Fig. 10(b)], where it is rather aggravated. Nevertheless, with the assistance of the Lyot filter, the AM is reduced by approximately 0.81 dB. This is beneficial for the output pulses [see Fig. 10(c)], at the expense of 2.7 dB amplification reduction. Finally, we have tested the Lyot filter against other challenging situations of this kind. Thus, we have found that the maximum AM at the SOA input which can be reduced by the Lyot filter below 1 dB is 4.8 dB.

D. IPDR of SOA-Lyot Filter System

Finally, we study whether the designed Lyot filter can increase the IPDR and accordingly the linear operation range of an SOA employed for direct signal amplification. This has been the ultimate goal of schemes that have exploited the concept of spectral elimination to suppress the SOA pattern effect [20], [24], [25], [31], [33]–[35]. Although in [33] we reported an estimate in the increase of the IPDR, this was done for a nonoptimized Lyot filter. In order to fully characterize the

capability of the Lyot filter to suppress the SOA pattern effect, it is necessary to address more accurately the improvement of the IDPR that is possible. This can be achieved by means of a systematic simulation analysis, and in this context, we note that the IPDR is associated with the achievement of error-free data amplification [45]. This was practically not possible with the bulk implementation of the Lyot filter due to the temperature dependence of the birefringence of its PMF [33]. Nevertheless, this technical difficulty can be overcome by adapting the tunable characteristics of the Lyot filter's transmission in a way that enhances its robustness against environmental changes. More specifically, the wavelength spacing (FSR) can be adjusted by replacing the standard PMF with a polarization maintaining (PM) photonic crystal fiber (PCF) and taking advantage of the exceptional insensitivity of its polarization properties to temperature. In fact, the temperature coefficient of birefringence for a PM-PCF is approximately 35 times smaller than that of an ordinary PMF at 1550 nm [46]. Thus, using a PM-PCF instead of a standard PMF can help achieve not only pattern-free but also error-free operation, at the expense of about six times increase in fiber cost [47]. Another efficient alternative is to employ a thermoelectric cooler for controlling and stabilizing the temperature of the conventional PMF [48]. It is also possible to achieve an equivalent effect by means of a programmable differential group delay line (DGDL) [37]. The relative delay introduced by the PMF, $\Delta\tau = BL/\mathrm{c}$, where c is the speed of light in vacuum, is 6.7 ps for the specified optimum PMF length of 5 m. This value is well supported by the operating range of commercial DGDLs [37]. Furthermore, the wavelength detuning $\Delta\lambda$ can be controlled if, instead of rotating the wave plates in Fig. 1, we employ an electrically driven phase modulator in between the two polarizers [49]. These options not only make the Lyot filter much more stable against external perturbations but also render it more compact for being incorporated with the SOA in the same module. Also, they allow the Lyot filter to be tuned in a fast, precise, flexible, and continuous manner. Thus, assuming that these solutions are adopted, we evaluate in the following the resultant improvement of the IPDR. Here, the IPDR is the range where the Q-factor, which is defined as $Q = [(P_1 - P_0)/(\sigma_1 + \sigma_0)]$, where P_1, P_0 and σ_1, σ_0 are the mean and standard deviation of the peak powers of the marks and spaces, respectively, is over 6 [39]. Since the ER between the marks and spaces is over 10 dB, even after the SOA, this means that $P_1 \gg P_0$, while the variations of the marks dominate over those of the spaces, so that $\sigma_1 \gg \sigma_0$. Then, the Q-factor is calculated in the thermal noise limit, where the amplitude fluctuations due to the pattern effect act as noise variance on the marks. The variation of the Q-factor after the SOA and after the Lyot filter for different peak input data powers is shown in Fig. 11(a). The curves have been obtained for $\tau = 175$ ps, which corresponds to a slower SOA gain recovery than that in the simulation analysis presented so far. The reason for doing this is that by definition, the Q-factor is calculated by taking into account the peak power of all bits in the PRBS. In contrast, the AM is calculated by taking into account only the maximum and minimum peak power of the marks. The consequence of this fact is that although the pulse amplitude fluctuations may

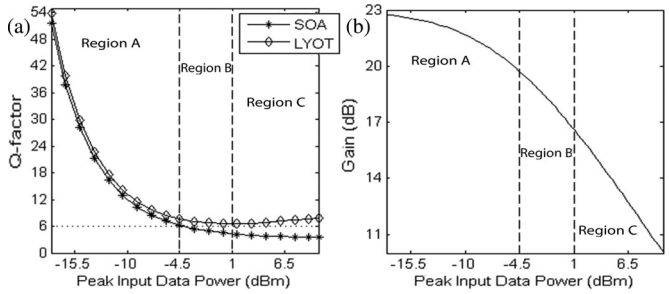

Fig. 11. (a) Variation of Q-factor as a function of different peak input data powers for SOA alone and with the connection of the optimized Lyot filter. The horizontal dotted line denotes the lower limit set for the Q-factor. (b) Instantaneous SOA gain variation versus peak input data power to define different saturation regions: A—low, B—medium, and C—deep.

be significant, they numerically tend to occur around the same average level and so the pattern effect appears to be less intense than it actually is. Thus, for $\tau = 75$ ps, which has been used to obtain the other simulation results, the AM after the SOA is 1.22 dB and hence unacceptable, but the Q-factor is 7.3 and thus acceptable. Therefore, although the AM quantifies correctly the pronounced pattern effect, the Q-factor underestimates it. In order to compensate for this inconsistency, the SOA gain recovery time must be higher so that the pattern effect is aggravated and the excursions between the pulse amplitudes across the whole amplified data stream cannot become statistically smoothened. In this manner, the SOA recovers its gain more slowly and accordingly the pattern effect is more intense. This in turn ensures that both AM and Q-factor are varied in the same direction, which allows us to evaluate correctly the IPDR.

The power levels considered in Fig. 11(a) define three saturation regions, which are illustrated in Fig. 11(b). These depend on the maximum extent that the instantaneous SOA gain of the mark after six consecutive spaces is dropped from its unsaturated value. Thus, saturation region A is characterized as "low" and the SOA gain is reduced up to 3 dB. Saturation region B is referred to as "medium" and the SOA gain is decreased by more than 3 dB. Saturation region C is termed as "deep" and the SOA gain is saturated by more than 6 dB. From Fig. 11(a), we see that in region A both SOA and Lyot curves are well above the Q-factor limit because there is no pattern effect. However, as the power is increased beyond –4.5 dBm and we enter region B, the pattern effect begins to manifest. This causes the drop of the SOA curve, which remains below the permissible Q-factor up to region C. This means that the maximum IPDR of the SOA is restricted to region A of low saturation, which obviously is not enough for the target applications of linear amplification. Nevertheless, with the addition of the Lyot filter, the Q-factor becomes acceptable across all regions A–C and the IPDR is increased. The same also holds for the OSNR, which is defined here as $\mathrm{OSNR} = P_1^2/\sigma_1^2$. This definition is consistent with the fact that in our model, we have neglected the contribution of amplified spontaneous emission (ASE) due to the SOA noise figure [5]. This assumption is valid since in practice an optical bandpass filter is placed at the SOA exit to remove noise [33]. Also, in the strong SOA gain saturation regime, where we aim

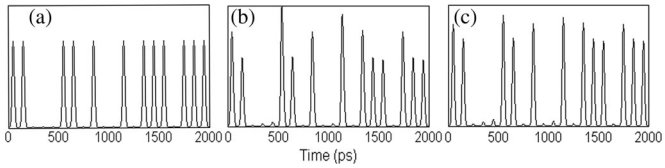

Fig. 12. Simulation results as in Fig. 7 but for slower SOA gain recovery, $\tau = 175$ ps.

at suppressing the pattern effect, the dynamical behavior of the SOA is mostly affected by the power of the data pulses and not of ASE. Then, the OSNR is linked to the Q-factor according to $\mathrm{OSNR} = Q^2$. This means that the improvement of the Q-factor after the Lyot filter compared to the SOA alone is also reflected on the OSNR. Thus, the OSNR of the SOA is increased by 6 dB for the specified optimum FSR and detuning of the Lyot filter. This OSNR enhancement is enabled because, under the given conditions of saturation and detuning, the SOA provides a gain that is sufficient for not allowing the signal quality to be degraded by Lyot filtering. Similar improvement of the OSNR has also been realized by other techniques used to suppress the pattern effect in direct signal amplification [20], [25]. Therefore, with the assistance of the Lyot filter, the SOA can support pattern-free operation even at high saturation level. This is shown in Fig. 12 for the same set of results as in Fig. 7 where, despite the quite demanding scenario with respect to the SOA gain recovery, the optimally designed Lyot filter manages to reduce the AM by 1.44 dB.

V. Conclusion

In conclusion, we have conducted a detailed characterization of a Lyot filter's capability to suppress the pattern effect in a SOA destined for direct signal amplification. The key tool in this effort has been the numerical model that we have applied to simulate the operation of the SOA-Lyot filter configuration. For this purpose, we have thoroughly investigated how to adjust and control the comb-like spectral response of the Lyot filter against a set of performance optimization criteria. By making the necessary tradeoffs between them, we have specified the allowable range and suitable choice of the Lyot filter parameters that determine decisively the achievement of this goal. Thus, we have found that the wavelength spacing must be 1.2 ± 0.35 nm and that the wavelength detuning must correspond to approximately one-sixth of this FSR. Under these conditions, we have demonstrated that the AM on the amplified data pulses is acceptable, the reduction in pulse amplification is tolerable, and the pulse original quality is preserved. Moreover, we have shown that the suggested design guarantees that the Lyot filter exhibits some further important features even under adverse operating conditions. These include the reduction of the AM on the data pulses that enter the SOA, the performance robustness against changes in the SOA parameters and longer PRBS, the restoration of the eye diagram's shape and ER, and the significant improvement of the IPDR. Finally, we have validated the derived simulation results by experiment.

References

[1] J. Mørk, M. L. Nielsen, and T. W. Berg, "The dynamics of semiconductor optical amplifiers: Modeling and applications," *Opt. Photon. News*, vol. 14, no. 7, pp. 42–48, Jul. 2003.

[2] S. Singh and Lovkesh, "Ultrahigh speed optical signal processing logic based on SOA-MZI," *IEEE J. Sel. Topics Quantum Electron.*, vol. 18, no. 9, pp. 970–977, Mar./Apr. 2012.

[3] S. Singh, "Performance comparison of optical network topologies in presence of optimized semiconductor optical amplifiers," *IEEE/OSA J. Opt. Commun. Netw.*, vol. 1, no. 4, pp. 313–323, Sep. 2009.

[4] D. R. Zimmerman and L. H. Spiekman, "Amplifiers for the masses: EDFA, EDWA, and SOA amplest for metro and access applications," *J. Lightw. Technol.*, vol. 22, no. 1, pp. 63–70, Jan. 2004.

[5] M. J. Connelly, *Semiconductor Optical Amplifiers*. Dordrecht, The Netherlands: Kluwer, 2002, ch. 6.

[6] Y. Kim, H. Jang, Y. Kim, J. Lee, D. Jang, and J. Jeong, "Transmission performance of 10-Gb/s 1550-nm transmitters using semiconductor optical amplifiers as booster amplifiers," *J. Lightw. Technol.*, vol. 21, no. 2, pp. 476–481, Feb. 2003.

[7] X. Wei, Y. Su, X. Liu, J. Leuthold, and S. Chandrasekhar, "10-Gb/s RZ-DPSK transmitter using a saturated SOA as a power booster and limiting amplifier," *IEEE Photon. Technol. Lett.*, vol. 16, no. 6, pp. 1582–1584, Jun. 2004.

[8] R. Gutiérrez-Castrejón and A. Filios, "Pattern-effect reduction using a cross-gain modulated holding beam in semiconductor optical in-line amplifier," *J. Lightw. Technol.*, vol. 24, no. 12, pp. 4912–4917, Dec. 2006.

[9] S. Boscolo, R. Bhamber, S. K. Turitsyn, V. K. Mezentsev, and V. S. Grigoryan, "RZ-DPSK transmission at 80 Gbit/s channel rate using in-line semiconductor optical amplifiers," *Opt. Commun.*, vol. 266, no. 2, pp. 656–659, Oct. 2006.

[10] R. Gutiérrez-Castrejón, L. Schares, and M. Duelk, "SOA nonlinearities in 4×25 Gb/s WDM pre-amplified system for 100-Gb/s Ethernet," *Opt. Quantum Electron.*, vol. 40, no. 13, pp. 1005–1019, Oct. 2008.

[11] S. Singh, "An approach to enhance the receiver sensitivity with SOA for optical communication systems," *Opt. Commun.*, vol. 284, no. 3, pp. 828–832, Feb. 2011.

[12] K. E. Zoiros, T. Siarkos, and C. S. Koukourlis, "Theoretical analysis of pattern effect suppression in semiconductor optical amplifier utilizing optical delay interferometer," *Opt. Commun.*, vol. 281, no. 14, pp. 3648–3657, Jul. 2008.

[13] C. S. Wong and H. K. Tsang, "Reduction of bit-pattern dependent errors from a semiconductor optical amplifier using an optical delay interferometer," *Opt. Commun.*, vol. 232, no. 1–6, pp. 245–249, 2004.

[14] N. Y. Kim, X. Tang, J. C. Cartledge, and A. K. Atieh, "Design and performance of an all-optical wavelength converter based on a semiconductor optical amplifier and delay interferometer," *J. Lightw. Technol.*, vol. 25, no. 12, pp. 3730–3738, Dec. 2007.

[15] M. T. Hill, H. de Waardt, G.-D. Khoe, and H. J. S. Dorren, "Short-pulse generation in interferometers employing semiconductor optical amplifiers," *IEEE J. Quantum Electron.*, vol. 39, no. 7, pp. 886–896, Jul. 2003.

[16] P. J. Winzer and R.-J. Essiambre, "Advanced modulation formats for high-capacity optical transport networks," *J. Lightw. Technol.*, vol. 24, no. 12, pp. 4711–4728, Dec. 2006.

[17] A. Mecozzi and J. Mørk, "Saturation induced by picosecond pulses in semiconductor optical amplifiers," *J. Opt. Soc. Amer. B*, vol. 14, no. 4, pp. 761–770, Apr. 1997.

[18] F. Girardin, G. Guekos, and A. Houbavlis, "Gain recovery of bulk semiconductor optical amplifier," *IEEE Photon. Technol. Lett.*, vol. 10, no. 6, pp. 784–786, Jun. 2008.

[19] R. Giller, R. J. Manning, G. Talli, and R. P. Webb, "Analysis of the dimensional dependence of semiconductor optical amplifier recovery speed," *Opt. Exp.*, vol. 15, no. 4, pp. 1773–1782, Feb. 2007.

[20] H. N. Tan, M. Matsuura, and N. Kishi, "Enhancement of input power dynamic range for multiwavelength amplification and optical signal processing in a semiconductor optical amplifier using holding beam effect," *J. Lightw. Technol.*, vol. 28, no. 17, pp. 2593–2602, Sep. 2010.

[21] C. Michie, A. E. Kelly, I. Armstrong, I. Andonovic, and C. Tombling, "An adjustable gain-clamped semiconductor optical amplifier (AGC-SOA)," *J. Lightw. Technol.*, vol. 25, no. 6, pp. 1466–1473, Jun. 2007.

[22] W. Zheng and G. W. Taylor, "CW gain characteristics of linear optical amplifiers," *IEEE J. Quantum Electron.*, vol. 43, no. 8, pp. 714–721, Aug. 2007.

[23] E. Ciaramella, A. D'Errico, and V. Donzella, "Using semiconductor-optical amplifiers with constant envelope WDM signals," *IEEE J. Quantum Electron.*, vol. 44, no. 5, pp. 403–409, May 2008.
[24] Q. Xu. M. Yao, Y. Dong, W. Cai, and J. Zhang, "Experimental demonstration of pattern effect compensation using an asymmetrical Mach-Zehnder interferometer with SOAs," *IEEE Photon. Technol. Lett.*, vol. 13, no. 12, pp. 1325–1327, Dec. 2001.
[25] K. Chan, C.-K. Chan, W. Hung, F. Tong, and L. K. Chen, "Waveform restoration in semiconductor optical amplifier using fiber loop mirror," *IEEE Photon. Technol. Lett.*, vol. 14, no. 7, pp. 995–997, Jul. 2002.
[26] A. V. Uskov, T. W. Berg, and J. Mørk, "Theory of pulse-train amplification without patterning effects in quantum-dot semiconductor optical amplifiers," *IEEE J. Quantum Electron.*, vol. 40, no. 3, pp. 306–320, Mar. 2004.
[27] L. Zhang, I. Kang, A. Bhardwaj, N. Sauer, S. Cabot, J. Jaques, and D. T. Neilson, "Reduced recovery time semiconductor optical amplifier using p-type-doped multiple quantum wells," *IEEE Photon. Technol. Lett.*, vol. 18, no. 22, pp. 2323–2325, Nov. 2006.
[28] K. Morito, "Output-level control of semiconductor optical amplifier by external light injection," *J. Lightw. Technol.*, vol. 23, no. 12, pp. 4332–4341, Dec. 2005.
[29] K. Inoue, "Optical filtering technique to suppress waveform distortion induced in a gain-saturated semiconductor optical amplifier," *Electron. Lett.*, vol. 33, no. 10, pp. 885–886, May 1997.
[30] T. Watanabe, H. Yasaka, N. Sakaida, and M. Koga, "Waveform shaping of chirp-controlled signal by semiconductor optical amplifier using Mach-Zehnder frequency discriminator," *IEEE Photon. Technol. Lett.*, vol. 10, no. 10, pp. 1422–1424, Oct. 1998.
[31] J. Yu and P. Jeppesen, "Increasing input power dynamic range of SOA by shifting the transparent wavelength of tunable optical filter," *J. Lightw. Technol.*, vol. 19, no. 9, pp. 1316–1325, Sep. 2001.
[32] J. Dong, X. Zhang, F. Wang, W. Hong, and D. Huang, "Experimental study of SOA-based NRZ-to-PRZ conversion and distortion elimination of amplified NRZ signal using spectral filtering," *Opt. Commun.*, vol. 281, no. 22, pp. 5618–5624, Nov. 2008.
[33] K. E. Zoiros, C. O'Riordan, and M. J. Connelly, "Semiconductor optical amplifier pattern effect suppression using Lyot filter," *Electron. Lett.*, vol. 45, no. 23, pp. 1187–1188, Nov. 2009.
[34] K. E. Zoiros, C. O'Riordan, and M. J. Connelly, "Semiconductor optical amplifier pattern effect suppression using a birefringent fiber loop," *IEEE Photon. Technol. Lett.*, vol. 22, no. 4, pp. 221–223, Feb. 2010.
[35] K. Hussain, R. Pradhan, and P. K. Datta, "Patterning characteristics and its alleviation in high bit rate amplification of bulk semiconductor optical amplifier," *Opt. Quantum. Electron.*, vol. 42, no. 1, pp. 29–43, Jan. 2010.
[36] G. P. Agrawal and N. A. Olsson, "Self-phase modulation and spectral broadening of optical pulses in semiconductor laser amplifiers," *IEEE J. Quantum Electron.*, vol. 25, no. 11, pp. 2297–2306, Nov. 1989.
[37] M. Wang, S. Fu, P. Shum, N. Q. Ngo, J. Wu, and J. Lin, "A tunable Lyot birefringent filter with variable channel spacing and wavelength using nonlinear polarization rotation in an SOA," *IEEE Photon. Technol. Lett.*, vol. 20, no. 18, pp. 1527–1529, Sep. 2008.
[38] K. E. Zoiros, Z. V. Rizou, and M. J. Connelly, "On the compensation of chirp induced from semiconductor optical amplifier on RZ data using optical delay interferometer," *Opt. Commun.*, vol. 284, no. 14, pp. 3539–3547, Jul. 2011.
[39] G. P. Agrawal, *Fiber-Optic Communication Systems*. New York, NY, USA: Wiley, 2002.
[40] F. J. MacWilliams and N. J. A. Sloane, "Pseudo-random sequences and arrays," *Proc. IEEE*, vol. 64, no. 12, pp. 1715–1729, Dec. 1976.
[41] R. Gutiérrez-Castrejón, L. Occhi, L. Schares, and G. Guekos, "Recovery dynamics of cross-modulated beam phase in semiconductor amplifiers and applications to all-optical signal processing," *Opt. Commun.*, vol. 195, no. 1–4, pp. 167–177, Aug. 2001.
[42] G. Gavioli, B. C. Thomsen, V. Mikhailov, and P. Bayvel, "Cascadability properties of optical 3R regenerators based on SOAs," *J. Lightw. Technol.*, vol. 25, no. 9, pp. 2766–2775, Sep. 2007.
[43] S. Singh and R. S. Kaler, "Transmission performance of 20 × 10 Gb/s WDM signals using cascaded optimized SOAs with OOK and DPSK modulation formats," *Opt. Commun.*, vol. 266, no. 1, pp. 100–110, Oct. 2006.
[44] S. V. Pato, R. Meleiro, D. Fonseca, P. André, P. Monteiro, and H. Silva, "All-optical burst-mode power equalizer based on cascaded SOAs for 10-Gb/s EPONs," *IEEE Photon. Technol. Lett.*, vol. 20, no. 24, pp. 2078–2080, Dec. 2008.
[45] R. Bonk, G. Huber, T. Vallaitis, S. Koenig, R. Schmogrow, D. Hillerkuss, R. Brenot, F. Lelarge, G.-H. Duan, S. Sygletos, C. Koos, W. Freude, and J. Leuthold, "Linear semiconductor optical amplifiers for amplification of advanced modulation formats," *Opt. Exp.*, vol. 20, no. 9, pp. 9657–9672, Apr. 2012.
[46] P. Man, N. Song, J. Jin, J. Song, and X. Xu, "Birefringence sensitivity to temperature of polarization maintaining photonic crystal fibers," *Opt. Laser Technol.*, vol. 44, no. 6, pp. 1829–1833, Sep. 2012.
[47] See for instance the relevant data sheets (2013). [Online]. Available: www.thorlabs.com
[48] C. W. Chow and H. K. Tsang, "Polarization-independent DPSK demodulation using a birefringent fiber loop," *IEEE Photon. Technol. Lett.*, vol. 17, no. 6, pp. 1313–1315, Jun. 2005.
[49] H. Q. Lam, P. Shum, L. N. Binh, and Y. Gong, "Electrically ultra-fast tunable optical filter employing HiBi fiber and phase modulator," *Opt. Commun.*, vol. 283, no. 13, pp. 2662–2664, Jul. 2010.

Zoe V. Rizou was born in Kozani, Greece, in 1986. She received the Diploma of Electrical and Computer Engineering from the Democritus University of Thrace (DUTH), Xanthi, Greece, in 2010. She received the M.Sc. degree for her work on semiconductor optical amplifier pattern effect suppression based on filtering schemes from the Department of Electrical and Computer Engineering, DUTH, where she is currently working toward the Ph.D. degree in microring resonators.

Her research interests include applications of microring resonators in optical communications.

Ms. Rizou is a member of the Technical Chamber of Greece.

Kyriakos E. Zoiros was born in Thessaloniki, Greece, in 1973. He received the Diploma of Electrical and Computer Engineering from the National Technical University of Athens, Athens, Greece, in 1996, where he received the Ph.D. degree in optical communications from the Photonics Communications Research Laboratory in 2000.

He is currently an Assistant Professor of optical communications in the Department of Electrical and Computer Engineering, Democritus University of Thrace, Xanthi, Greece. In spring 2009, he was on leave at the University of Limerick in Ireland doing experimental work on semiconductor optical amplifier (SOA) pattern effect suppression techniques at the Optical Communications Research Group. He is the author or coauthor of more than 60 international journal and conference papers as well as of three book chapters. His current research interests include conventional as well as quantum-dot SOA devices, circuits and subsystems, applications of microring resonators in optical communications, microwave photonics, and free space optical communications.

Antonios Hatziefremidis (S'96–M'00) was born in Chalkis, Greece, in 1972. He received the diploma of electrical and computer engineering from the National Technical University of Athens, Athens, Greece, in 1995, where he received the Ph.D. degree in optical communications from the Photonics Communications Research Laboratory in 1999.

He is currently an Associate Professor in the Department of Aircraft Technology, Technological Educational Institute, Chalkis, Greece. In 2001, he joined Hellenic Aerospace Industry, initially in the Research and Development Department, and latter on in the Satellite Communications and Applications Department. His research interests include optical amplifiers, optical switching networks, multiwavelength continuous-wave and pulsed laser sources for wavelength-division multiplexing and optical time-division multiplexing, optical wireless access and satellite communications.

Michael J. Connelly (S'89–M'92) received the Ph.D. degree in electronic engineering from the National University of Ireland, Dublin, Ireland, in 1992.

He is a Senior Lecturer in electronic engineering and the Director of the Optical Communications Research Group, University of Limerick, Limerick, Ireland. The current research interests of his group include semiconductor optical amplifiers, fiber ring lasers, and optical coherence tomography.